Roles of TOG and jelly-roll domains of centrosomal protein CEP104 in its functions in cilium elongation and Hedgehog signaling

Received for publication, March 4, 2020, and in revised form, August 11, 2020 Published, Papers in Press, August 20, 2020, DOI 10.1074/jbc.RA120.013334

Takashi Yamazoe[1,‡], **Tomoaki Nagai**[1,2,‡,*], **Shinya Umeda**[1], **Yuko Sugaya**[1], **and Kensaku Mizuno**[1,3,*]

From the [1]*Department of Molecular and Chemical Life Sciences, Graduate School of Life Sciences, Tohoku University, Sendai, Miyagi, Japan, the* [2]*Department of Biochemistry, Fukushima Medical University School of Medicine, Fukushima, Japan, and the* [3]*Institute of Liberal Arts and Sciences, Tohoku University, Kawauchi, Sendai, Miyagi, Japan*

Primary cilia are generated through the extension of the microtubule-based axoneme. Centrosomal protein 104 (CEP104) localizes to the tip of the elongating axoneme, and *CEP104* mutations are linked to a ciliopathy, Joubert syndrome. Thus, CEP104 has been implicated in ciliogenesis. However, the mechanism by which CEP104 regulates ciliogenesis remains elusive. We report here that CEP104 is critical for cilium elongation but not for initiating ciliogenesis. We also demonstrated that the tumor-overexpressed gene (TOG) domain of CEP104 exhibits microtubule-polymerizing activity and that this activity is essential for the cilium-elongating activity of CEP104. Knockdown/rescue experiments showed that the N-terminal jelly-roll (JR) fold partially contributes to cilium-elongating activity of CEP104, but neither the zinc-finger region nor the SXIP motif is required for this activity. CEP104 binds to a centriole-capping protein, CP110, through the zinc-finger region and to a microtubule plus-end–binding protein, EB1, through the SXIP motif, indicating that the binding of CP110 and EB1 is dispensable for the cilium-elongating activity of CEP104. Moreover, CEP104 depletion does not affect CP110 removal from the mother centriole, which suggests that CEP104 functions after the removal of CP110. Last, we also showed that CEP104 is required for the ciliary entry of Smoothened and export of GPR161 upon Hedgehog signal activation and that the TOG domain plays a critical role in this activity. Our results define the roles of the individual domains of CEP104 in its functions in cilium elongation and Hedgehog signaling and should enhance our understanding of the mechanism underlying *CEP104* mutation–associated ciliopathies.

Primary cilia are antenna-like protrusions that emanate from the surface of most vertebrate cells, and these structures consist of a microtubule (MT)-based axoneme that extends from a basal body and a ciliary membrane that envelopes the axoneme (1, 2). Primary cilia are generally formed when a cell exits from the cell cycle and enters the quiescent phase (1, 2). At the onset of ciliogenesis, the mother centriole is translocated to the plasma membrane and converted into the basal body, from which axonemal MTs extend. Two centrosomal proteins, CP110 and CEP97, localize at the distal ends of both mother and daughter centrioles and block axonemal MT assembly, and thus the removal of CP110 and CEP97 from the mother centriole is essential for initiating axoneme extension and ciliogenesis (3–7). Subsequently, the axoneme extends and ciliary components are transported into the cilia by the intraflagellar transport (IFT) system (8, 9).

The IFT system recruits various types of ion channels and receptors to the ciliary membrane (10–12), and this allows primary cilia to serve as cellular antennae that sense and transmit diverse chemical signals, including Hedgehog (Hh) and Wnt, and mechanical signals (13–15). Thus, primary cilia play crucial roles in the development and homeostasis of several tissues, and defects in the formation of primary cilia lead to various types of human disorders, collectively termed ciliopathies, that present a complex set of symptoms, including neuronal and retinal degeneration, polycystic kidney, situs inversus, and polydactyly (16, 17). Genetic studies of ciliopathies and knockdown-based screening have identified many genes involved in ciliogenesis, but the molecular mechanisms underlying ciliogenesis and the etiology of ciliopathies remain largely unknown (16, 17).

Joubert syndrome (JBTS) is an autosomal recessive ciliopathy that causes mid- and hind-brain hypotrophy, frequently accompanied by ataxia, oculomotor apraxia, retinal dystrophy, nephronophthisis, and liver fibrosis (18). JBTS-associated genes encode the proteins that localize to the tip, transition zone, and membrane of cilia (19–23), and most of these proteins are essential for the regulation of Hh signaling. Accordingly, mutations of these genes frequently cause abnormalities in the ciliary transport of Hh-related transmembrane proteins (19–21, 24–26).

Centrosomal protein 104 (CEP104), an evolutionarily conserved protein, is encoded by *CEP104*, which was recently reported to be a causative gene for JBTS (27, 28). CEP104 binds to CP110 and CEP97 and colocalizes with these proteins at the distal ends of both mother and daughter centrioles in nonciliated cells (29, 30). When cells are growth-arrested, CEP104 on the mother centriole is dissociated from the CP110-CEP97 complex and transferred to the tip of the elongating axoneme (30, 31), and depletion of CEP104 causes the loss or shortening of the cilia (30). These findings strongly suggest that CEP104 plays a critical role in ciliogenesis. However, the mechanism by which CEP104 regulates ciliogenesis remains elusive.

CEP104 contains a jelly-roll fold (JR fold; also termed IFT25-like fold) at the N terminus, a tumor-overexpressed gene

This article contains supporting information.
[‡]These authors contributed equally to this work.
*For correspondence: Tomoaki Nagai, tnagai@fmu.ac.jp; Kensaku Mizuno, kmizuno@biology.tohoku.ac.jp.

(TOG) domain in the central region, and four tandem zinc-finger (ZF) repeats and an S*X*IP motif in the C-terminal region (32, 33). CEP104 was recently reported to bind to CEP97 and CSPP1 (another JBTS-associated protein, named for centrosome and spindle pole–associated protein 1) through the JR domain, tubulins through the TOG domain, CP110 and NIMA-related kinase-1 (NEK1) through the ZF region, and end-binding protein-1 (EB1) through the S*X*IP motif (29, 32–34). These results suggest that by interacting with the aforementioned proteins, CEP104 can potentially regulate multiple steps in ciliogenesis, such as the conversion of the mother centriole into the basal body through its interaction with CP110 and CEP97, and the extension of the axoneme through the interaction with tubulins and EB1. However, the precise function of CEP104 at the distinct stages of ciliogenesis and the roles of the individual domains in CEP104 localization and function are unknown.

Here, we show that CEP104 is essential for the elongation of the ciliary axoneme but is not involved in the initiation of cilium formation. We provide evidence that the TOG domain of CEP104 exhibits MT-polymerizing activity and that this activity is essential for cilium elongation. We also show that the N-terminal JR fold partially contributes to the cilium-elongating activity of CEP104, but neither the C-terminal ZF region nor the S*X*IP motif is necessary for this activity, which indicates that the cilium-elongating activity of CEP104 does not require its binding to CP110, NEK1, or EB1. A recent study showed that the CEP104 mutation suppresses ciliary import of Smoothened (Smo) upon Hh signal activation (34). We here demonstrate that CEP104 is required for ciliary import of Smo and export of G-protein–coupled receptor 161 (GPR161) in Hh signal transduction and that the TOG domain of CEP104 plays a critical role in this activity.

Results

Knockdown of CEP104 shortens cilia but does not affect frequency of cilium formation

To investigate the role of CEP104 in ciliogenesis, we first examined the effects of *CEP104* knockdown on the formation and length of primary cilia. Human telomerase reverse transcriptase-immortalized retinal pigment epithelial-1 (RPE1) cells were transfected with *CEP104*-targeting siRNAs and cultured under serum-starved conditions. Immunoblotting of the cell extracts revealed that two independent siRNAs effectively suppressed CEP104 expression (Fig. 1*A*). To examine the population of ciliated cells and the length of cilia, cells were immunostained with an anti-acetyl (Ac)-tubulin antibody (Fig. 1*B*). Quantification of the results showed that whereas *CEP104* knockdown exerted no apparent effect on the population of ciliated cells (Fig. 1*C*), the knockdown significantly shortened primary cilia (Fig. 1, *B* and *D*). The average ± S.D. lengths of primary cilia were 2.79 ± 0.65 μm in control cells and 1.66 ± 0.52 and 1.80 ± 0.49 μm in *CEP104*-knockdown cells (Fig. 1*D*). These results indicate that CEP104 functions in cilium elongation but is not involved in triggering cilium formation. In accordance with our results, a recent study showed that *CEP104* silencing reduces the cilium length in Kupffer's vesicle in zebrafish (34).

CEP104 TOG domain promotes MT polymerization

To examine the mechanism by which CEP104 promotes the cilium elongation, we analyzed the function of the TOG domain in the central region of CEP104 (Fig. 2*A*). TOG domains are recognized to bind to tubulins and regulate MT dynamics (35), and the CEP104 TOG domain was recently shown to exhibit tubulin-binding ability (32, 33). However, whether the TOG domain of CEP104 can promote MT polymerization has remained unknown. To address this question, recombinant CEP104 TOG domain was expressed in *Escherichia coli* and purified (Fig. 2, *A* and *B*) and used in *in vitro* assays in which MT polymerization was measured by monitoring tubulin solution turbidity; the analysis revealed that the CEP104 TOG domain effectively promotes MT polymerization (Fig. 2*C*). For this analysis, we also constructed a mutant form of the CEP104 TOG domain, W448A/V493D/R626A (WA/VD/RA), in which three amino acid residues predicted to participate in tubulin binding (32, 33) were point-mutated (Fig. 2, *A* and *B*), and analyzed its MT-polymerizing activity. In the *in vitro* assay, the WA/VD/RA mutant of the CEP104 TOG domain showed decreased MT-polymerizing activity (Fig. 2*C*). Thus, the TOG domain of CEP104 has the ability to promote MT polymerization, and this depends on the domain's tubulin-binding activity.

MT-polymerizing activity of TOG domain is required for cilium-elongating activity of CEP104

We next investigated the role of the MT-polymerizing activity of the TOG domain in the cilium-elongating activity of CEP104; we constructed plasmids encoding yellow fluorescent protein (YFP)-tagged, siRNA-resistant (*sr*) WT CEP104 and its TOG domain mutant (WA/VD/RA) and used these in knockdown/rescue experiments. Immunoblot analysis confirmed the expression of CEP104(WT)-YFP and its WA/VD/RA mutant (Fig. 2*D*). In control YFP-expressing cells, treatment with *CEP104* siRNA caused cilium shortening, but the siRNA effect was rescued in cells expressing CEP104(WT) (Fig. 2, *E* and *F*), indicating that the cilium shortening occurred due to CEP104 depletion and not any off-target effect of *CEP104* siRNA. By contrast, expression of the WA/VD/RA mutant did not rescue the cilium shortening induced by *CEP104* siRNA (Fig. 2, *E* and *F*), indicating that the MT-polymerizing activity of the TOG domain is essential for the cilium-elongating activity of CEP104. Fluorescence image analyses showed that CEP104(WT)-YFP and its WA/VD/RA mutant localize to the ciliary base and axoneme (Fig. S1), suggesting that the tubulin binding is not required for ciliary localization of CEP104.

EB1 binding is not required for ciliary tip localization and cilium-elongating activity of CEP104

CEP104 was previously shown to bind to EB1 through an S*X*IP motif (SKIP, amino acids 905–908) located near the C terminus of CEP104 (29). In *Chlamydomonas* and human epithelial cells, EB1 and EB3 are reported to localize to the basal body and the tip of cilia (36, 37), and CEP104 also localizes to the tip of cilia (31); this raised the possibility that EB1 participates in CEP104 localization to the ciliary tip. To test this, we treated RPE1 cells with an *EB1*-targeting siRNA, which effectively

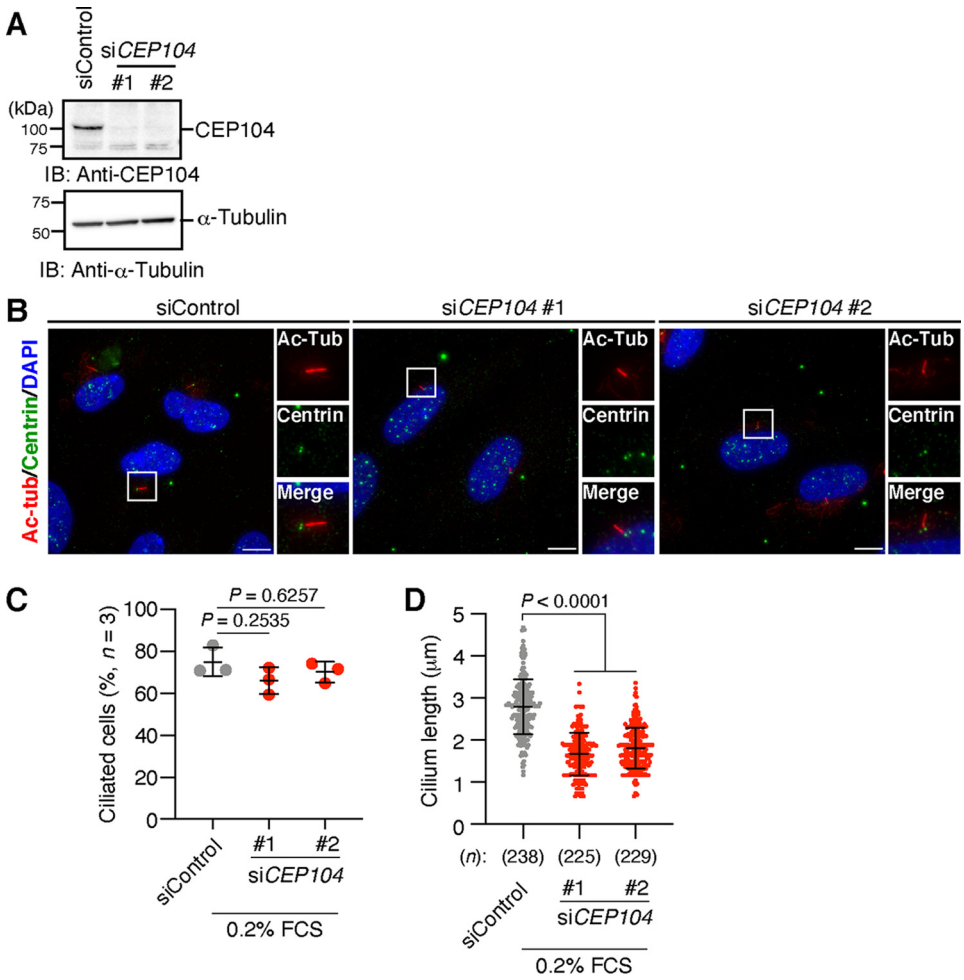

Figure 1. *CEP104* knockdown shortens cilia but exerts no effect on frequency of cilium formation. *A*, immunoblot analysis of the knockdown efficiency of *CEP104* siRNAs. RPE1 cells were transfected with control or *CEP104*-targeting siRNAs and cultured for 48 h, and then cell lysates were immunoblotted with the indicated antibodies. *B*, effects of *CEP104* knockdown on cilium formation and length. RPE1 cells were transfected with control or *CEP104* siRNAs, serum-starved for 48 h, fixed, and immunostained with anti-Ac-tubulin (*red*) and anti-centrin (*green*) antibodies. DNA was stained with DAPI (*blue*). *Scale bar*, 10 μm. *Magnified images* of *boxed regions* are shown on the *right*. *C*, quantification of the percentage of ciliated cells, based on staining of Ac-tubulin. *Lines* and *error bars* show means and S.D. from three independent experiments. In each experiment, more than 50 cells were analyzed. *D*, quantification of cilium length in ciliated cells, based on staining of Ac-tubulin. *Dot plots* indicate cilium length of individual cells. *Lines* and *error bars* show means and S.D. (*n* = total number of cells used for measuring cilium length). *p* values were calculated by ordinary one-way ANOVA followed by Tukey's test.

suppressed EB1 protein expression (Fig. 3*A*). In cells transfected with a control siRNA, immunostaining with an anti-CEP104 antibody revealed that CEP104 localizes to the two (daughter and mother) centrioles in nonciliated cells and to the ciliary tip and a single (daughter) centriole in ciliated cells. Unexpectedly, *EB1* knockdown exerted no marked effect on CEP104 localization in either nonciliated or ciliated cells (Fig. 3*B*), which suggests that EB1 is not involved in the localization of CEP104 to the ciliary tip.

To examine whether EB1 binding contributes to the cilium-elongating function of CEP104, we constructed a CEP104 mutant, in which the SKIP sequence (amino acids 905–908) was replaced with SKNN (Fig. 3*C*). Co-precipitation assays revealed that EB1 binds to CEP104(WT) but not the SKNN mutant (Fig. 3*D*), which confirmed that EB1 binds to CEP104 through the SKIP sequence. We next analyzed whether expression of YFP-tagged CEP104(WT) or its SKNN mutant affects ciliary length in *CEP104*-knockdown cells. Immunoblotting confirmed the expression of CEP104(WT)-YFP and its SKNN mutant (Fig. 3*E*). The results of knockdown/rescue experiments showed that the cilium shortening induced by *CEP104* knockdown was rescued to a similar level by the expression of the WT and the SKNN mutant of CEP104 (Fig. 3, *F* and *G*). Thus, the binding of EB1 is not essential for the cilium-elongating activity. Fluorescence image analysis showed that CEP104(SKNN)-YFP localizes to the ciliary base and axoneme (Fig. S1), further suggesting that the EB1 binding is not required for ciliary localization of CEP104.

CEP104 is not involved in CP110 removal from mother centriole

CP110 localizes on the distal ends of both mother and daughter centrioles and suppresses inadequate ciliogenesis by blocking ciliary axoneme extension in proliferating cells (4). Upon serum starvation, CP110 is removed from the mother centriole, which results in axoneme extension and cilium formation (4). Intriguingly, CEP104 binds to and colocalizes with CP110 at the mother and daughter centrioles in serum-fed cells, and upon serum starvation, CP110 is removed from the mother

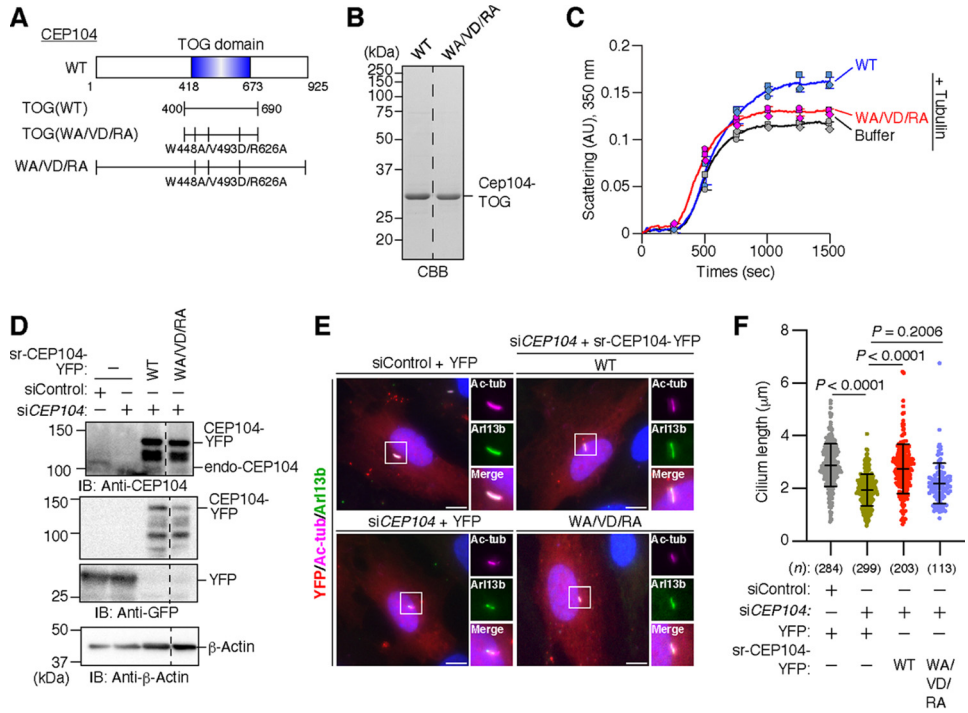

Figure 2. CEP104 TOG domain exhibits MT-polymerizing activity, and this activity is required for cilium-elongating activity of CEP104. *A*, schematic representation of CEP104 and its mutants. *Numbers* indicate amino acid residues. *B*, purification of CEP104 TOG domain and its mutant. Recombinant GST-CEP104 TOG proteins expressed in *E. coli* were bound to GSH-Sepharose, and GST was removed using PreScission Protease. Purified proteins were analyzed using SDS-PAGE and CBB staining. *C*, *in vitro* MT polymerization assay. Purified tubulin (12.5 μM) was incubated at 37 °C in the absence (buffer) or presence of each of 2 μM TOG domain protein of CEP104 (WT) or WA/VD/RA mutant. Kinetics of tubulin polymerization was measured based on turbidity at 350 nm. *AU*, arbitrary unit. *Lines* and *error bars* show means and S.D. from three independent experiments. Dot plots indicate the turbidity in each experiment. *D*, expression of CEP104-YFP and its mutant in *CEP104*-depleted cells. RPE1 cells were co-transfected with *CEP104* siRNA and CEP104-YFP or its WA/VD/RA mutant and cultured for 48 h. Cell lysates were immunoblotted with anti-CEP104, anti-GFP, and anti-β-actin antibodies. *E*, CEP104(WT), but not CEP104(WA/VD/RA), rescues cilium shortening in *CEP104*-depleted cells. RPE1 cells were co-transfected with *CEP104* siRNA and CEP104-YFP or its WA/VD/RA mutant, serum-starved for 48 h, fixed, and then immunostained with anti-Ac-tubulin (*magenta*) and anti-Arl13b (*green*) antibodies. DNA was stained with DAPI (*blue*). Cells were also imaged by YFP fluorescence (*red*). *Scale bar*, 10 μm. *Magnified images* of *boxed regions* are shown on the *right*. *F*, quantification of cilium length in ciliated cells, based on Ac-tubulin staining. Dot plots indicate the cilium length of individual cells. *Lines* and *error bars* show means and S.D. (*n* = total number of cells used for measuring cilium length). *p* values were calculated by ordinary one-way ANOVA followed by Tukey's test.

centriole, and the CEP104 localized on the mother centriole is dissociated from CP110 and translocated to the tip of the elongating cilium (30, 38). In accord with these findings, the results of co-precipitation analyses showed that CEP104 was associated with CP110 under serum-fed conditions but dissociated from CP110 under serum-starved conditions (Fig. 4*A*).

Because CEP104 interacts with CP110 at centrioles, CEP104 could potentially function in CP110 removal from the mother centriole. To test this possibility, we analyzed the effect of *CEP104* knockdown on serum starvation–induced CP110 removal from the mother centriole. RPE1 cells were treated with *CEP104* siRNAs, serum-starved, and then stained with antibodies against CP110, Ac-tubulin, and γ-tubulin. In 67% of control cells, CP110 was localized to a single centriole (Fig. 4, *B* and *C*), which indicated CP110 removal from the mother centriole in these cells, and the percentage of cells with CP110 localized to a single centriole was unaffected by *CEP104* knockdown (Fig. 4, *B* and *C*). This result suggests that CEP104 is not involved in serum starvation–induced CP110 removal from the mother centriole.

Effects of double knockdown of CEP104 and CP110 on cilium formation and length

To further investigate the functional relationship between CEP104 and CP110, we examined the effects of double knockdown of *CEP104* and *CP110* on cilium formation and length in serum-fed RPE1 cells by Ac-tubulin staining, and we compared these effects with those in *CEP104* or *CP110* single-knockdown cells. Treatment with *CP110* siRNA effectively suppressed CP110 expression (Fig. 4*D*), and, as reported (4), *CP110* single knockdown significantly increased the population of ciliated cells under the serum-supplemented conditions (Fig. 4, *E* and *F*). Ac-tubulin–positive structures formed by *CP110* knockdown were co-stained with Arl13b and IFT88 (Fig. S2), indicating that they are the *bona fide* cilia but not the elongated centrioles, which were previously reported in nonciliated U2OS and extraembryonic endoderm stem (XEN) cells (39–42). Notably, *CEP104* knockdown did not affect the number of ciliated cells in the case of either control or *CP110*-knockdown cells (Fig. 4, *E* and *F*), which indicates that CEP104 neither promotes nor suppresses the inhibitory function of CP110 in ciliogenesis. Furthermore, whereas *CEP104* single knockdown led to significant ciliary shortening, concurrent knockdown of *CP110* did not additionally affect ciliary length in *CEP104*-knockdown cells (Fig. 4, *E* and *G*); this indicates that CP110 is not involved in the function of CEP104 in cilium elongation. Thus, CP110 and CEP104 function independently in cilium formation and elongation,

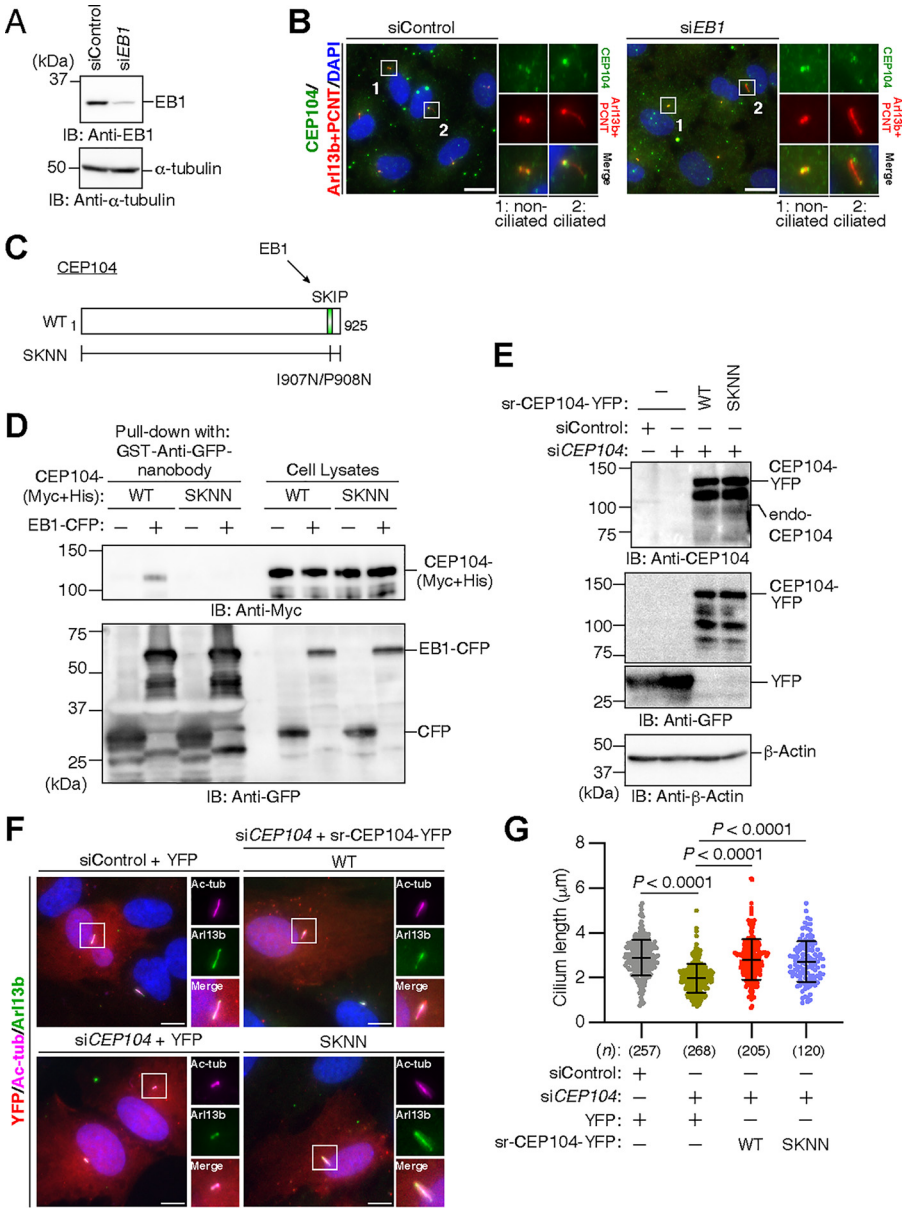

Figure 3. EB1 binding is not required for ciliary tip localization and cilium-elongating activity of CEP104. *A*, immunoblot analysis of knockdown efficiency of *EB1* siRNA. RPE1 cells were transfected with control or *EB1*-targeting siRNA and cultured for 48 h, and cell lysates were immunoblotted with anti-EB1 and anti-α-tubulin antibodies. *B*, *EB1* knockdown does not affect CEP104 localization at ciliary tip. RPE1 cells were transfected with control or *EB1* siRNA, serum-starved for 48 h, fixed, and immunostained with anti-CEP104 (*green*), anti-Arl13b, and anti-pericentrin (*red*) antibodies. DNA was stained with DAPI (*blue*). *Scale bar*, 20 μM. *Magnified images* of *boxed regions* are shown on the *right*. *C*, schematic representation of CEP104 and its SKNN mutant. *Numbers* indicate amino acid residues. *D*, CEP104(SKNN) does not bind to EB1. HEK293T cells were co-transfected with CEP104-(Myc+His) and EB1-CFP (cyan fluorescent protein). Cell lysates were immunoprecipitated with GST-tagged anti-GFP-nanobody, prebound to GSH-Sepharose beads. Precipitates and lysates were immunoblotted with anti-GFP and anti-Myc antibodies. *E*, expression of CEP104-YFP or its SKNN mutant in *CEP104*-depleted cells. RPE1 cells were co-transfected with *CEP104* siRNA and CEP104(WT) or its SKNN mutant and cultured for 48 h. Cell lysates were immunoblotted with anti-CEP104, anti-GFP, and anti-β-actin antibodies. *F*, CEP104(WT) and its SKNN mutant rescue cilium shortening in *CEP104*-depleted cells. RPE1 cells were co-transfected with *CEP104* siRNA and CEP104-YFP or its SKNN mutant, serum-starved for 48 h, fixed, and then stained with anti-Ac-tubulin (*magenta*) and anti-Arl13b (*green*) antibodies. DNA was stained with DAPI (*blue*). Cells were also imaged by YFP fluorescence (*red*). *Scale bar*, 10 μm. *Magnified images* of *boxed regions* are shown on the *right*. *G*, quantification of cilium length in ciliated cells. Dot plots indicate the cilium length of individual cells. *Lines* and *error bars* show means and S.D. (*n* = total number of cells used for measuring cilium length). *p* values were calculated by ordinary one-way ANOVA followed by Tukey's test.

respectively, and CEP104 functions in promoting cilium elongation after CP110 removal from the mother centriole.

JR fold, but not ZF region, is involved in cilium-elongating activity of CEP104

CEP104 was shown to bind to CEP97 and CSPP1 through its N-terminal JR fold (amino acids 1–163) and to CP110 and NEK1 through the C-terminal ZF region (amino acids 730–887) (32–34). To examine the roles of the JR fold and ZF region in the cilium-elongating activity of CEP104, we constructed and tested two CEP104 deletion mutants: ΔJR (Δ1–164), lacking the JR fold, and ΔZF (Δ731–886), lacking the ZF region (Fig. 5*A*). The results of co-precipitation assays confirmed that CEP97 binds to CEP104-WT and ΔZF but not ΔJR (Fig. 5*B*)

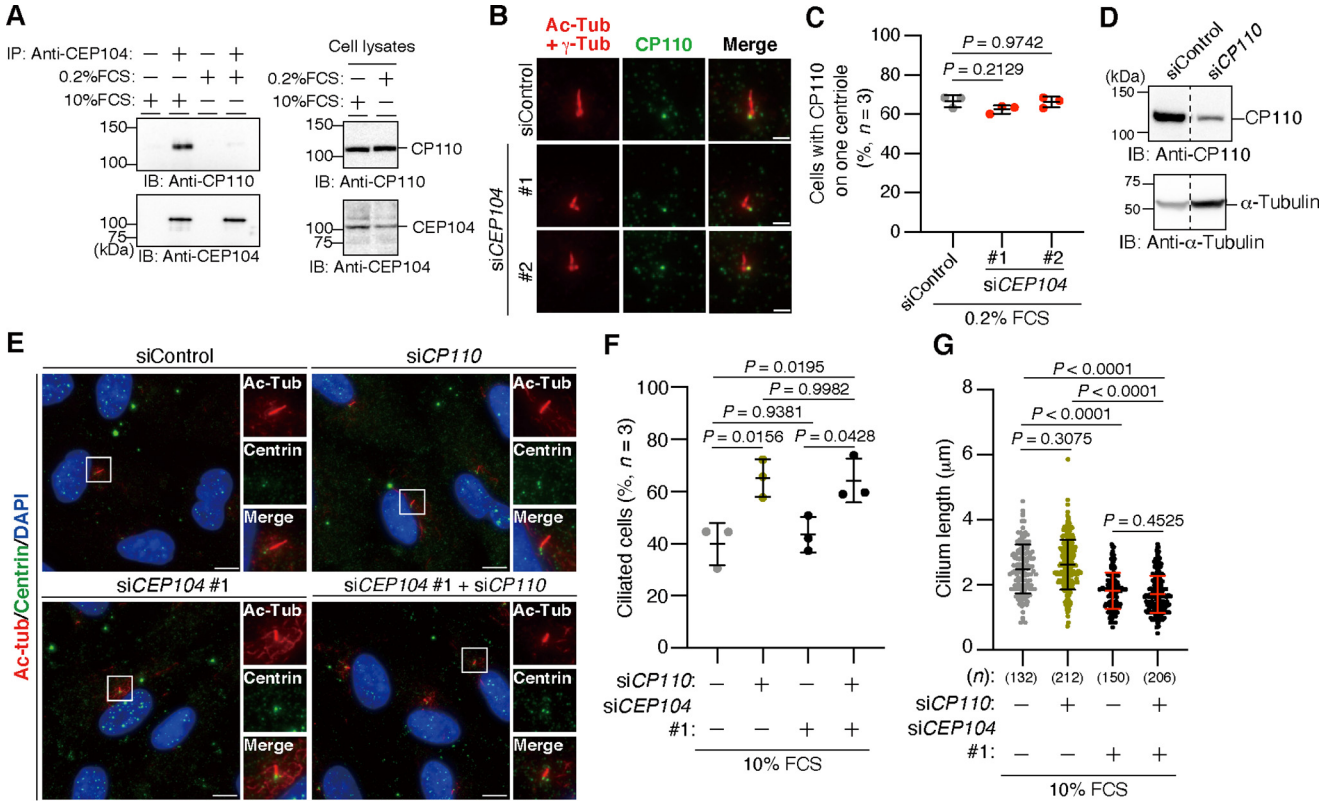

Figure 4. CEP104 is not involved in CP110 removal from mother centriole, and effects of *CEP104* and *CP110* double knockdown on cilium formation and length. *A*, dissociation of CEP104 from CP110 upon serum starvation. RPE1 cells were cultured under serum-fed (10% FCS) or serum-starved (0.2% FCS) conditions for 48 h. Cell lysates were immunoprecipitated with anti-CEP104 antibody, and precipitates and lysates were immunoblotted with the indicated antibodies. *B*, effect of *CEP104* knockdown on CP110 removal from mother centriole. RPE1 cells were transfected and serum-starved for 48 h, fixed, and stained with anti-Ac-tubulin and anti-γ-tubulin antibodies (*red*) and anti-CP110 antibody (*green*). *Scale bar*, 2 μm. *C*, quantification of cells with CP110 localized on one centriole. Plots indicate the individual experimental values. *Lines* and *error bars* show means and S.D. from three independent experiments. In each experiment, more than 50 cells were analyzed. *D*, immunoblot analysis of knockdown efficiency of *CP110* siRNA. RPE1 cells were transfected with control or *CP110*-targeting siRNA and cultured for 48 h, and cell lysates were immunoblotted with the indicated antibodies. *E*, effects of single or double knockdown of *CEP104* and *CP110* on frequency of ciliated cells and cilium length. RPE1 cells were individually or concomitantly transfected with *CEP104* and *CP110* siRNAs, cultured for 48 h in medium containing 10% FCS, fixed, and then immunostained with anti-Ac-tubulin (*red*) and anti-centrin (*green*) antibodies. DNA was stained with DAPI (*blue*). *Scale bar*, 10 μm. *Magnified images* of *boxed regions* are shown on the *right*. *F*, quantification of the population of ciliated cells. Dot plots indicate individual experimental values. *Lines* and *error bars* show means and S.D. from three independent experiments. In each experiment, more than 50 cells were analyzed. *G*, quantification of cilium length in ciliated cells. Dot plots indicate cilium length of individual cells. *Lines* and *error bars* show means and S.D. (*n* = total number of cells used for measuring cilium length). *p* values were calculated by ordinary one-way ANOVA followed by Tukey's test.

and that CP110 and NEK1 bind to CEP104-WT and ΔJR but not ΔZF (Fig. 5, *C* and *D*). Next, we analyzed the rescue effects of the expression of YFP-tagged CEP104(WT) or its deletion mutants on cilium length in *CEP104*-knockdown cells. Immunoblotting results confirmed the expression of CEP104(WT)-YFP and its ΔJR and ΔZF mutants (Fig. 5*E*). Expression of CEP104(WT) or its ΔZF mutant almost fully rescued the cilium-shortening effect produced by *CEP104* siRNA (Fig. 5, *F* and *G*). On the other hand, the rescue effect of CEP104(ΔJR) was modest and significantly weaker than that of CEP104(WT) (Fig. 5, *F* and *G*). Similarly, it was reported that the cells bearing the N-terminally truncated *CEP104* mutant exhibited the shortened cilium (34). These results suggest that the N-terminal JR fold contributes, at least in part, to the cilium-elongating activity of CEP104, whereas the C-terminal ZF region and the binding of CP110 and NEK1 are dispensable for the function of CEP104 in cilium elongation. Fluorescence image analyses showed that CEP104(ΔJR) and CEP104(ΔZF) localize to the ciliary base and axoneme (Fig. S1), suggesting that neither the JR fold nor the ZF region is required for ciliary localization of CEP104.

CEP104 binding is not required for ciliogenesis-suppressing activity of CP110

Our aforementioned results showed that CP110 is not involved in the cilium-elongating function of CEP104; we examined here whether CEP104 is involved in the CP110 function of suppressing ciliogenesis. We constructed a deletion mutant, CP110(Δ907–937), which lacks CEP104-binding ability (33) (Fig. 6*A*), and by performing co-precipitation assays, we confirmed that this mutant had lost the CEP104-binding activity (Fig. 6*B*). We next tested the effect of overexpression of CP110(WT) or CP110(Δ907–937) on serum starvation-induced ciliogenesis. Under serum starvation, 70% of control YFP-expressing cells were ciliated, but in cells overexpressing either CP110(WT) or CP110(Δ907–937), the serum starvation–induced ciliogenesis was significantly suppressed (with only 13 and 12% of the cells being ciliated,

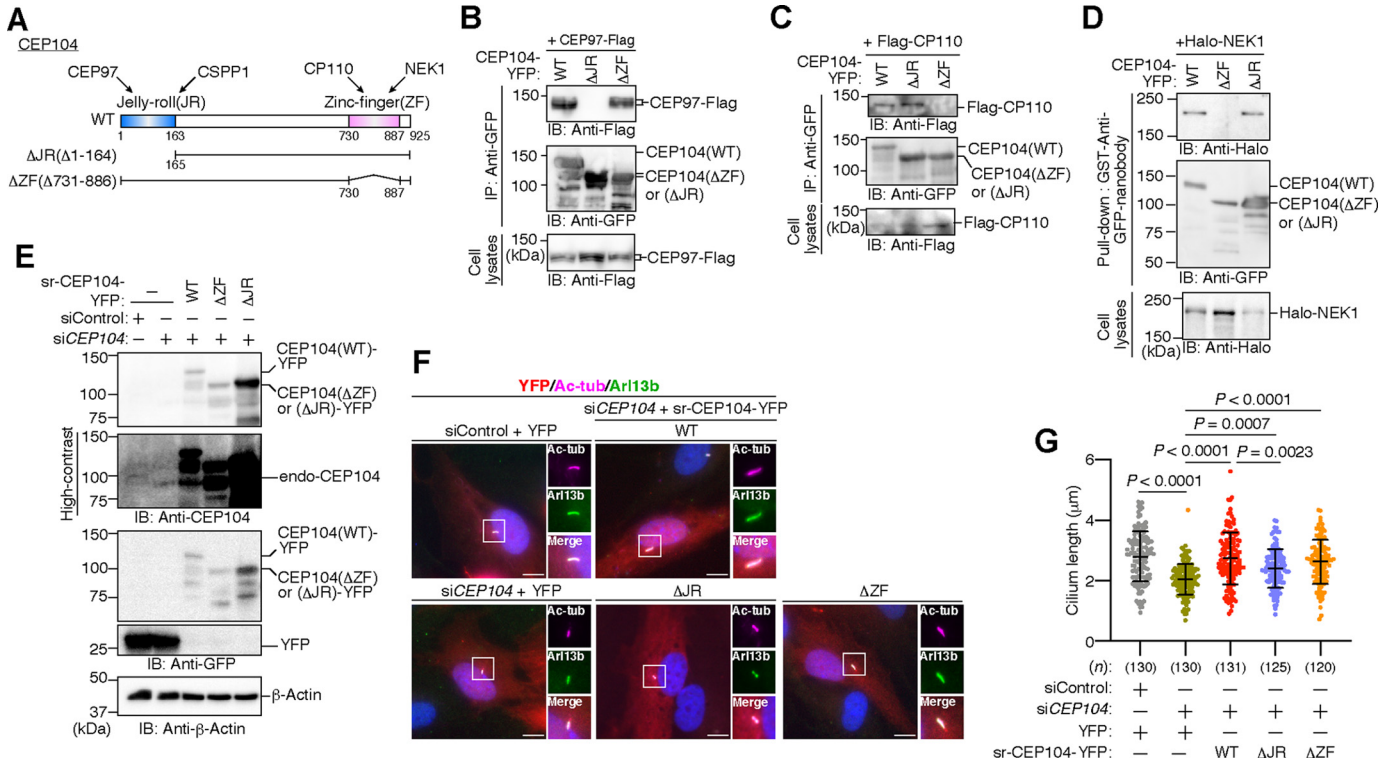

Figure 5. CEP104 JR fold, but not ZF region, is required for cilium-elongating activity of CEP104. *A*, schematic representation of CEP104 and its ΔJR and ΔZF mutants. *Numbers* indicate amino acid residues. *B*, CEP97 does not bind to CEP104(ΔJR). HEK293T cells were co-transfected with CEP97-FLAG and CEP104-YFP or its ΔJR or ΔZF mutant. Cell lysates were immunoprecipitated with anti-GFP antibody, and precipitates and lysates were immunoblotted with anti-FLAG and anti-GFP antibodies. *C*, CP110 does not bind to CEP104(ΔZF). HEK293T cells were co-transfected with FLAG-CP110 and CEP104-YFP or its mutants. Cell lysates were immunoprecipitated with anti-GFP antibody, and precipitates and lysates were immunoblotted with anti-FLAG and anti-GFP antibodies. *D*, NEK1 does not bind to CEP104(ΔZF). HEK293T cells were co-transfected with Halo-NEK1 and CEP104-YFP or its mutants. Cell lysates were immunoprecipitated with GST-tagged anti-GFP-nanobody, prebound to GSH-Sepharose beads, and precipitates and lysates were immunoblotted with anti-Halo and anti-GFP antibodies. *E*, expression of CEP104-YFP and its mutants in *CEP104*-depleted cells. RPE1 cells were co-transfected with *CEP104* siRNA and CEP104-YFP or its ΔZF or ΔJR mutant and cultured for 48 h. Cell lysates were immunoblotted with anti-CEP104, anti-GFP, and anti-β-actin antibodies. *F*, CEP104(WT) and (ΔZF), but not (ΔJR), rescue cilium shortening in *CEP104*-depleted cells. RPE1 cells were co-transfected with *CEP104* siRNA and CEP104-YFP or its mutants, serum-starved for 48 h, fixed, and then stained with anti-Ac-tubulin (*magenta*) and anti-Arl13b (*green*) antibodies. DNA was stained with DAPI (*blue*). Cells were also imaged by YFP fluorescence (*red*). *Scale bar*, 10 μm. *Magnified images* of *boxed regions* are shown on the *right*. *G*, quantification of cilium length in ciliated cells, based on Ac-tubulin staining. Dot plots indicate cilium length of individual cells. *Lines* and *error bars* show means and S.D. (*n* = total number of cells used for measuring cilium length). *p* values were calculated by ordinary one-way ANOVA followed by Tukey's test.

respectively) (Fig. 6, *C* and *D*). This result suggests that CP110 suppresses ciliogenesis independently of CEP104 binding.

CEP104 is required for Hh signal–induced ciliary trafficking of Smo and GPR161 and GLI1 expression

Mutations in *CEP104* are linked to JBTS (27, 28). Intriguingly, mutations in JBTS-related genes are typically associated with abnormalities of Hh signaling caused by enhanced or reduced ciliary trafficking of Hh signal-related transmembrane proteins, such as Smo and GPR161 (19–21, 24–26). A recent study showed that CEP104 mutation suppresses ciliary Smo accumulation upon Hh signal activation (34). To further investigate the role of CEP104 in the ciliary control of Hh signaling and JBTS pathogenesis, we examined the effect of *CEP104* knockdown on the ciliary entry of Smo upon Hh signal activation. Serum-starved RPE1 cells were treated with a Smo agonist (SAG) (43) and immunostained with an anti-Smo antibody. Whereas SAG treatment almost tripled the fluorescence intensity of ciliary Smo immunostaining in control cells (Fig. 7, *A* and *B*), the relative intensity of ciliary Smo was markedly lower in SAG-treated *CEP104*-knockdown cells than in SAG-treated control siRNA-treated cells (Fig. 7, *A* and *B*). These results suggest that CEP104 is required for the Hh signal–induced ciliary entry of Smo.

To further examine the role of CEP104 in the ciliary trafficking of Hh-related proteins, we tested the effect of *CEP104* knockdown on SAG-induced ciliary exit of GPR161, a receptor that is reported to localize to the ciliary membrane in the absence of Hh signal but to be removed from cilia upon Hh-signal activation (44, 45). Accordingly, SAG treatment caused a reduction in the fluorescence intensity of ciliary GPR161 in control siRNA–transfected cells (Fig. 7, *C* and *D*). Notably, after *CEP104* knockdown, the intensity of ciliary GPR161 was significantly increased in both untreated and SAG-treated cells (Fig. 7, *C* and *D*). These results suggest that CEP104 plays a role in the export of GPR161 from cilia in both unstimulated and Hh signal–stimulated cells.

To investigate the function of CEP104 in regulating Hh signaling, we analyzed the effect of *CEP104* knockdown on the expression of the Hh-target gene *GLI1*. Quantitative PCR analyses of SAG-treated and -untreated cells revealed that *GLI1* mRNA level was significantly increased after SAG treatment in control cells but not in *CEP104*-knockdown cells (Fig. 7*E*) and

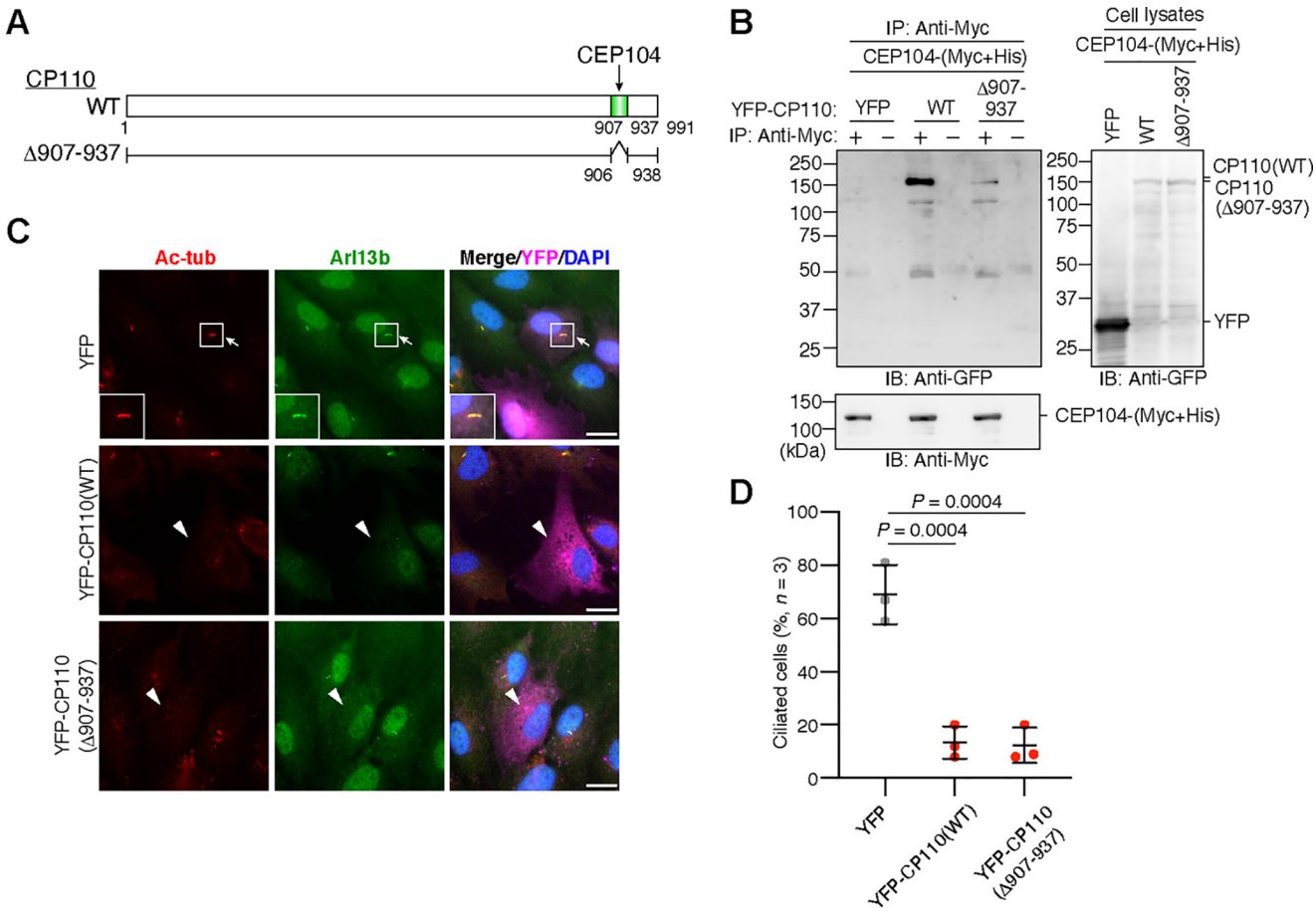

Figure 6. CEP104 binding is not required for CP110 suppression of serum starvation–induced ciliogenesis. *A*, schematic representation of CP110 and its Δ907-937 mutant. *Numbers* indicate amino acid residues. *B*, CP110(Δ907–937) does not bind to CEP104. HEK293T cells were co-transfected with CEP104-(Myc+His) and YFP-CP110 or its mutant. Cell lysates were immunoprecipitated with anti-Myc antibody, and precipitates and lysates were immunoblotted with anti-Myc and anti-GFP antibodies. *C*, overexpression of CP110 or its Δ907–937 mutant suppresses serum starvation–induced ciliogenesis. RPE1 cells were transfected with YFP, YFP-CP110(WT), or YFP-CP110(Δ907–937) and serum-starved for 48 h. Cells were fixed and immunostained with anti-Ac-tubulin (*red*) and anti-Arl13b (*green*) antibodies. DNA was stained with DAPI (*blue*). Cells were also imaged by YFP fluorescence (*magenta*). *Scale bar*, 10 μm. Magnified images of one Ac-tubulin– and Arl13b–positive primary cilium (*arrows*, *top row*) in a control YFP-expressing cell are shown in the *bottom left inset*. *Arrowheads* (*middle* and *bottom rows*) indicate YFP-positive nonciliated cells. *D*, quantification of the population of ciliated cells among YFP-positive cells. Dot plots indicate the individual experimental values. *Lines* and *error bars* show means and S.D. from three independent experiments. In each experiment, more than 100 cells were analyzed. *p* values were calculated by ordinary one-way ANOVA followed by Tukey's test.

further that SAG-induced *GLI1* gene expression was significantly lower in *CEP104*-knockdown cells than in control cells (Fig. 7*E*). These results indicate that CEP104 plays a critical role in the cilium-mediated Hh signal transduction.

Last, we investigated the roles of the TOG and JR domains of CEP104 in Hh signaling by knockdown/rescue experiments. Expression of CEP104(WT) and CEP104(ΔJR), but not CEP104 (WA/VD/RA), rescued the defects in SAG-induced ciliary entry of Smo and exit of GPR161 in *CEP104*-knockdown cells (Fig. 7, *F* and *G*), indicating that the TOG domain is critical, but the JR fold is dispensable, for the function of CEP104 in Hh signal–induced ciliary trafficking of Smo and GPR161.

Discussion

CEP104 has been previously shown to bind to and colocalize with two centriolar capping proteins, CP110 and CEP97, on the distal ends of both mother and daughter centrioles in nonciliated cells (29, 30). In response to cell-cycle exit signals, CP110 and CEP97 are removed from the mother centriole, and CEP104 on the mother centriole is dissociated from these two proteins and translocated to the tip of the elongating cilium (29, 30, 38). The removal of CP110 and CEP97 is a key step required to initiate cilium extension, and CEP104 binds to these proteins at the distal ends of centrioles; therefore, CEP104 was proposed to play a role in ciliogenesis by affecting the centriolar-capping activity of CP110 and CEP97 or the removal of the two proteins from the mother centriole (29, 30). However, we showed here that *CEP104* depletion exerts no effect on CP110 removal from the mother centriole and further that a CP110 mutant (Δ907–937) lacking CEP104-binding ability suppresses ciliogenesis to a similar extent as WT CP110. Thus, CEP104 is involved in neither the centriolar removal of CP110 nor the centriolar-capping activity of CP110. Our results also showed that *CEP104* depletion shortens cilia but does not significantly alter the frequency of ciliated cells. A recent study also showed that CEP104 mutation significantly reduces axoneme length (34). Together, these findings suggest that CEP104 does not participate in the initiation of cilium formation but preferentially functions at the stage of axoneme elongation

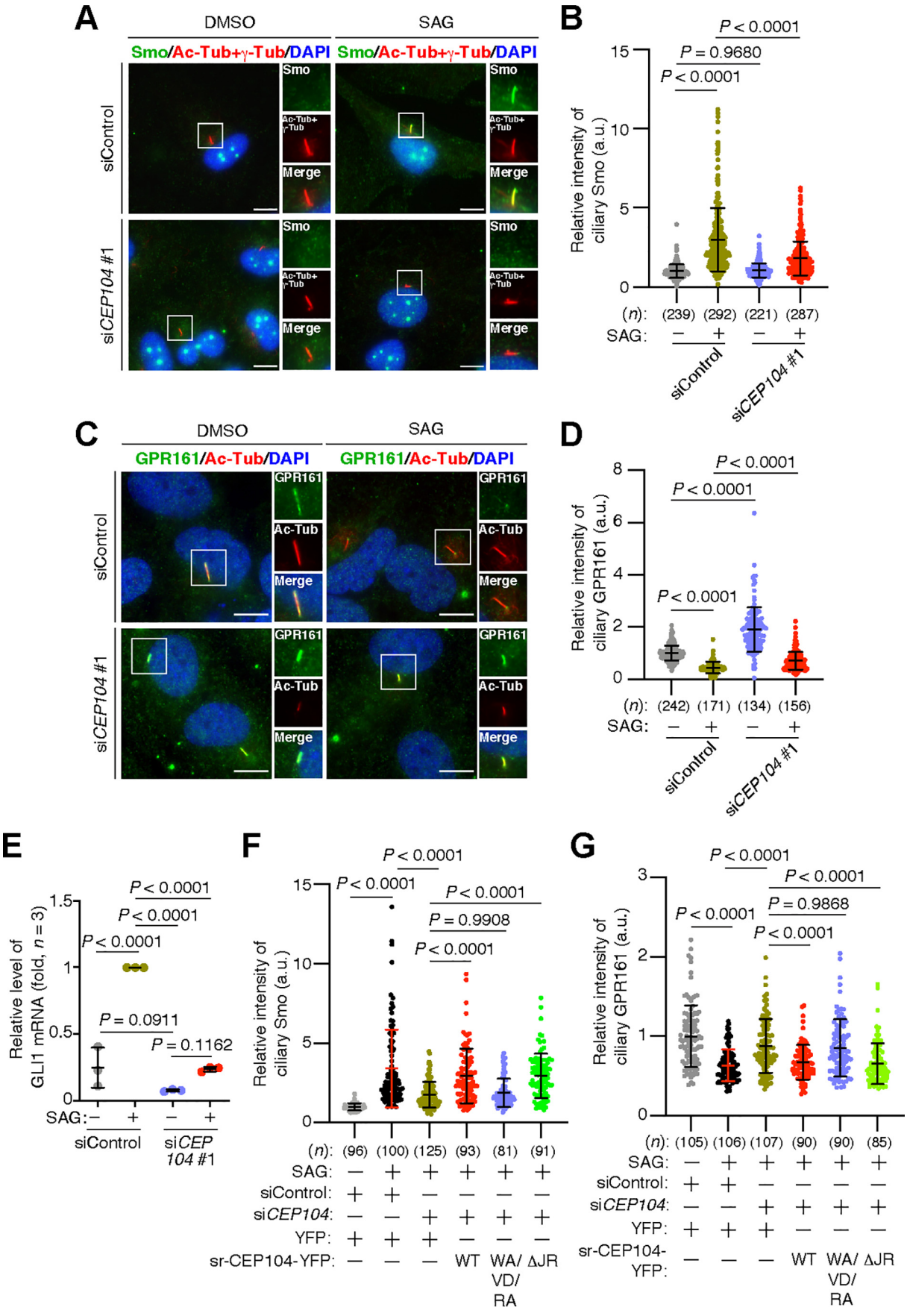
A
DMSO
SAG
Smo/Ac-Tub+γ-Tub/DAPI
Smo/Ac-Tub+γ-Tub/DAPI
siControl
siCEP104 #1
Smo
Ac-Tub+γ-Tub
Merge
B
P < 0.0001
P = 0.9680
P < 0.0001
Relative intensity of ciliary Smo (a.u.)
15
10
5
0
(n): (239) (292) (221) (287)
SAG: − + − +
siControl
siCEP104 #1
C
DMSO
SAG
GPR161/Ac-Tub/DAPI
GPR161/Ac-Tub/DAPI
siControl
siCEP104 #1
GPR161
Ac-Tub
Merge
D
P < 0.0001
P < 0.0001
P < 0.0001
Relative intensity of ciliary GPR161 (a.u.)
8
6
4
2
0
(n): (242) (171) (134) (156)
SAG: − + − +
siControl
siCEP104 #1
E
P < 0.0001
P < 0.0001
P < 0.0001
P = 0.0911
P = 0.1162
Relative level of GLI1 mRNA (fold, n = 3)
1.5
1
0.5
0
SAG: − + − +
siControl
siCEP 104 #1
F
P < 0.0001
P < 0.0001
P < 0.0001
P = 0.9908
P < 0.0001
Relative intensity of ciliary Smo (a.u.)
15
10
5
0
(n): (96) (100) (125) (93) (81) (91)
SAG: − + + + + +
siControl: + + − − − −
siCEP104: − − + + + +
YFP: + + + − − −
sr-CEP104-YFP: − − − WT WA/VD/RA ΔJR
G
P < 0.0001
P < 0.0001
P < 0.0001
P = 0.9868
P < 0.0001
Relative intensity of ciliary GPR161 (a.u.)
3
2
1
0
(n): (105) (106) (107) (90) (90) (85)
SAG: − + + + + +
siControl: + + − − − −
siCEP104: − − + + + +
YFP: + + + − − −
sr-CEP104-YFP: − − − WT WA/VD/RA ΔJR

after the CP110-CEP97 complex is removed from the mother centriole.

We investigated the roles of the individual domains of CEP104 in its function in cilium elongation by knockdown/rescue experiments. CEP104(ΔZF), which does not bind to either CP110 or NEK1, and CEP104(SKNN), which does not bind to EB1, retain the ability to promote cilium elongation; these results suggest that the interactions with CP110, NEK1, and EB1 are not involved in the cilium-elongating activity of CEP104. By contrast, the rescue effect of CEP104(ΔJR) was modest and significantly weaker than that of CEP104(WT), which suggests that the N-terminal JR fold plays some role in this activity. CSPP1 and CEP97 interact with CEP104 through the N-terminal JR fold–containing region (33, 34). CSPP1 is a JBTS-associated gene product that colocalizes with CEP104 at the tip of cilia, and *CSPP1* depletion induces cilium shortening (34), which suggests the possibility that the interaction with CSPP1 through the N-terminal JR fold–containing region is involved in the cilium-elongating activity of CEP104.

TOG domains are generally recognized to bind to tubulins and regulate MT dynamics (35). Recently, the crystal structure of the TOG domain of CEP104 was solved and its tubulin-binding activity was demonstrated (32, 33). Here, we first showed that the purified TOG domain of CEP104 exhibits MT-polymerizing activity in cell-free assays, and then that mutation of the TOG domain at three key residues involved in tubulin binding impairs the domain's MT-polymerizing activity in cell-free assays and abolishes the cilium-elongating activity of CEP104 in cells. These results indicate that the tubulin-binding and MT-polymerizing activities of the TOG domain are essential for the cilium-elongating activity of CEP104.Whereas most TOG domain-harboring proteins, such as XMAP215, contain tandem repeats of TOG domains and regulate MT dynamics by means of multiple TOG domains (35), CEP104 harbors only one TOG domain. Intriguingly, a single TOG domain (TOG2) of CLASP was recently shown to hold the potential to suppress MT catastrophes (46). Thus, similar to TOG2 of CLASP, the single TOG domain of CEP104 might mediate CEP104-promoted MT polymerization. CEP104 also binds to EB1— which can potentially recruit binding proteins to MT plus-ends—through the S*X*IP motif located near the C terminus, but our results showed that EB1 binding is dispensable for CEP104 localization and function. Moreover, a recent study showed that CSPP1 is not required for CEP104 localization to the ciliary tip (34). We also showed that all mutations introduced in this study have no apparent effect on ciliary localization of CEP104. Thus, further studies are required to enhance our understanding of the molecular mechanisms underlying the MT-polymerizing activity of the TOG domain of CEP104 and the localization of CEP104 at the ciliary tip.

CEP104 was previously shown to be a causative gene for JBTS (27, 28), and mutations of other JBTS-associated genes, such as *ARL13B*, cause defects in Hh signaling (47). We have provided evidence here that CEP104 is critical for the control of cilium-dependent Hh signaling. Our results agree with the recently reported findings from a CRISPR-based screening of genes involved in Hh signaling (48, 49) and a functional analysis of *CEP104* in cultured cells and zebrafish (34). We showed that *CEP104* knockdown suppressed the ciliary entry of Smo and the exit of GPR161; this suggests that *CEP104* depletion causes defects in Hh signaling through not only the shortening of cilia, but also the disruption of normal ciliary trafficking.

Knockdown/rescue experiments revealed that expression of CEP104(WT), but not its TOG domain mutant, rescues the defects in SAG-induced ciliary Smo/GPR161 translocation in *CEP104* knockdown cells, indicating that the TOG domain plays a critical role in the function of CEP104 in ciliary Smo/GPR161 trafficking upon Hh signal activation. In contrast, expression of CEP104(ΔJR) almost fully restored the defects in ciliary Smo/GPR161 translocation in *CEP104*-knockdown cells, indicating that the JR fold is dispensable for the function of CEP104 in ciliary Smo/GPR161 trafficking. However, considering that our data are based on the result of overexpression of CEP104(ΔJR), we cannot exclude the possibility that the JR fold has some role in the function of CEP104 in Hh signaling and overexpression of CEP104(ΔJR) compensates for its functional attenuation. In this respect, a recent study showed that the N-terminally deleted mutation of CEP104 strongly suppresses SAG-induced ciliary entry of Smo (34). Inconsistent results may reflect the differences in their "Experimental Procedures" and the length of deleted region of CEP104 mutants used in these two studies; our study used the overexpression of CEP104 (ΔJR) (lacking the N-terminal 164 amino acids) in *CEP104*-knockdown cells, whereas the previous study used the CRISPR-Cas9 system to edit endogenous *CEP104* gene to its mutant gene (lacking the N-terminal 203 amino acids) (34). Taken together, these results suggest that the N-terminal JR fold–containing region of CEP104 plays some role in Smo trafficking.

Figure 7. Knockdown/rescue experiments of *CEP104* on ciliary transport of Smo and GPR161 and expression of *GLI1* transcript. *A*, *CEP104* knockdown blocks SAG-induced Smo entry into cilia. RPE1 cells were transfected with control or *CEP104* siRNA, serum-starved for 48 h, and then treated with DMSO or 200 nM SAG for 24 h. Cells were then fixed and immunostained with anti-Ac-tubulin (*red*), anti-γ-tubulin (*red*), and anti-Smo (*green*) antibodies. DNA was stained with DAPI (*blue*). *Scale bar*, 10 μm. *Magnified images* of *boxed regions* are shown on the *right*. *B*, quantification of the relative fluorescence intensity of Smo in primary cilia. Dot plots indicate individual experimental values. *Lines* and *error bars* show means and S.D. (*n* = total number of cells used for measuring Smo intensity). *C*, *CEP104* knockdown increases ciliary GPR161 in untreated and SAG-treated cells. RPE1 cells were transfected and treated as in *A*, after which the cells were fixed and immunostained with anti-Ac-tubulin (*red*) and anti-GPR161 (*green*) antibodies. DNA was stained with DAPI (*blue*). *Scale bar*, 10 μm. *Magnified images* of *boxed regions* are shown on the *right*. *D*, quantification of the relative fluorescence intensity of GPR161 in primary cilia. Dot plots indicate individual experimental values. *Lines* and *error bars* show means and S.D. (*n* = total number of cells used for measuring GPR161 intensity). *E*, effect of *CEP104* knockdown on *GLI1* mRNA expression in untreated and SAG-treated cells. RPE1 cells were transfected and treated as in *A*. Total RNAs were isolated and subject to real-time quantitative PCR analysis. The amounts of PCR products for *GLI1* were normalized against those for *UBC*, and then -fold changes were normalized to the value of control siRNA–transfected and SAG-treated cells. Dot plots indicate individual experimental values. *Lines* and *error bars* show means and S.D. from three independent experiments. *F*, quantification of the relative fluorescence intensity of Smo in cilia. Dot plots indicate individual experimental values. *Lines* and *error bars* show means and S.D. (*n* = total number of cells used for measuring Smo intensity). *G*, quantification of the relative fluorescence intensity of GPR161 in cilia. Dot plots indicate individual experimental values. *Lines* and *error bars* show means and S.D. (*n* = total number of cells used for measuring GPR161 intensity). *p* values were calculated by ordinary one-way ANOVA followed by Tukey's test.

Further studies are required to define the roles of the JR fold and the following region (165–203 amino acids) for the function of CEP104 in Smo/GPR161 trafficking and Hh signaling.

A bioinformatics study predicted that the JR fold of CEP104 is structurally related to IFT25 (32). IFT25 and its binding partner IFT27 form a subcomplex of IFT-B and are essential for ciliary Hh signaling (50, 51), and, interestingly, recombinant CEP104 was recently shown to interact with IFT27 (34). Thus, CEP104 could function in the trafficking of Hh signal–related ciliary membrane proteins by regulating the activity of the IFT machinery.

In conclusion, we showed that CEP104 plays a crucial role in cilium elongation and that this requires the MT-polymerizing activity of the TOG domain. We also showed that CEP104 plays an essential role in Hh signaling by regulating the ciliary trafficking of Smo and GPR161. Further investigation into CEP104 functions and regulation mechanisms will contribute to enhanced understanding of the pathogenesis of ciliopathies.

Experimental procedures

Antibodies and reagents

The following antibodies/reagents were purchased: rabbit polyclonal antibodies against EB1 (BD Biosciences #610534, 1:500 for Western blotting (WB)), Arl13b (Proteintech #17711-1-AP, 1:1000 for immunofluorescence (IF)), pericentrin (BioLegend #923701, 1:1000 for IF), GFP (Thermo Fisher Scientific #A6455, 1:2000 for WB and immunoprecipitation (IP)), GPR161 (Proteintech #13398-1-AP, 1:1000 for IF), CP110 (Bethyl #A301-343A, 1:250 for IF and WB), and Halo tag (Promega #G9281, 1:1000 for WB); mouse monoclonal antibodies against CEP104 (Abnova #H00009371-B01P, 1:1000 for WB, IF, and IP), Smoothened (E-5, Santa Cruz Biotechnology #sc-166685, 1:200 for IF), Ac-α-tubulin (6-11B-1, MilliporeSigma #T7451, 1:1000 for IF), Myc tag (PL14, Medical and Biological Laboratories #M047-3, 1:1000 for WB and IP), α-tubulin (B-5-1-2, MilliporeSigma #5168, 1:1000 for WB), γ-tubulin (GTU-88, MilliporeSigma #5326, 1:250 for IF), β-actin (AC15, MilliporeSigma #A1978, 1:1000 for WB), and FLAG epitope (M2, MilliporeSigma #F3165, 1:1000 for WB); Alexa Fluor 488–/568–labeled anti-mouse IgG (#A11029 and #A11031, respectively) and anti-rabbit IgG (#A11034 and #A11036) and Alexa Fluor 633–labeled anti-rabbit IgG (#A21071) secondary antibodies (1:2000 for IF; Thermo Fisher Scientific); 4′,6-diamino-2-phenylindole (DAPI; Polyscience #09224); SAG (Abcam #ab142160); and tubulin purified from porcine brain (Cytoskeleton #T240-A).

Plasmid construction

CEP104 cDNA was cloned through PCR amplification, and cDNAs for EB1, CP110, and glutathione *S*-transferase (GST)-GFP-nanobody were provided by T. Inoue (Johns Hopkins University), B. D. Dynlacht (New York University), and K. Nakayama (Kyoto University), respectively. A plasmid encoding Halo-NEK1 was purchased from Promega (#FHC01183). Mutations in CEP104 were generated using a site-directed mutagenesis kit (Agilent #200519). The *sr-CEP104* cDNAs were constructed by introducing six silent mutations into a target sequence of *CEP104* siRNA (5′-GGTCGAACGCTGCCGCATA-3′).

siRNAs

The siRNA-targeting sequences were as follows: 5′-GGUGGAGAGAUGUCGAAUA-3′ (*CEP104* siRNA #1, Thermo Fisher Scientific), 5′-CGCUAGAUGACUUAGCUUU-3′ (*CEP104* siRNA #2, Thermo Fisher Scientific), 5′-GGACAUCCUAUACGAACU-3′ (*CP110* siRNA, GE Healthcare), and 5′-AAUGAGUCUCUGCAGUUGAA-3′ (*EB1* siRNA, Thermo Fisher Scientific).

Cell culture and transfection

RPE1 cells (a gift from H. Nakanishi, Kumamoto University) were cultured in Dulbecco's modified Eagle's medium/Ham's F-12 (Wako Pure Chemical #042-30555) supplemented with 10% fetal calf serum (FCS) (CosmoBio #CCP-FBS-BR-500). HEK293T cells were purchased from ATCC (#CRL-3216) and cultured in Dulbecco's modified Eagle's medium containing 10% FCS. Plasmids were transfected using FuGENE HD (Promega #E231A) or JetPEI (PolyPlus #101-40N).

RPE1 cells were transfected with plasmids and siRNAs by using Lipofectamine LTX with PLUS reagent (Thermo Fisher Scientific #15338100) and Lipofectamine RNAi MAX (Thermo Fisher Scientific #13778150), respectively. For *EB1*/*CEP104*/*CP110* knockdown experiments, RPE1 cells were plated on coverslips in 6-well culture plates and transfected with the corresponding siRNAs, cultured for 24 h, and then serum-starved for 48 h before fixation. For knockdown/rescue experiments, RPE1 cells were plated on coverslips in 6-well culture plates, transfected with plasmids, cultured for 4 h, transfected with *CEP104* siRNAs, cultured for 20 h, and then serum-starved for 48 h before fixation.

Immunofluorescence and fluorescence microscopy

RPE1 cells were washed with PBS and then fixed/permeabilized by treating with 4% paraformaldehyde for 5 min at 37 °C followed by methanol for 15 min at −20 °C, with 4% paraformaldehyde for 30 min at 37 °C followed by 0.1% Triton X-100 for 5 min at room temperature, with 4% paraformaldehyde for 30 min at 37 °C followed by 1% SDS for 5 min and 0.1% Triton X-100 for 5 min at room temperature or with methanol alone. Cells were blocked with 2% FCS in PBS (30 min) and incubated with primary antibodies diluted in Can Get Signal immunostain solution A (Toyobo #NKB-501) (1 h at room temperature or overnight at 4 °C) and then with secondary antibodies diluted in 2% FCS/PBS (1 h at room temperature). DNA was stained with 0.5 μg/ml DAPI (5 min) and mounted in embedding medium (100 mM Tris-HCl, pH 7.4, 1 mg/ml *p*-phenylenediamine, and 90% glycerol). Fluorescence images were obtained using a DMI 6000B fluorescence microscope (Leica Microsystems) equipped with a PL Apo ×63 oil objective lens (numerical aperture 1.3) and CCD camera (Cool SNAP HQ, Roper Scientific) and an A1 confocal microscope (Nikon) with a ×60 objective lens (numerical aperture 1.27). ImageJ software (National Institutes of Health) was used for Z-stack projection and measurement of cilium length.

Immunoprecipitation

HEK293T cells were lysed in lysis buffer (150 mM NaCl, 50 mM HEPES, pH 7.5, 1% Nonidet P-40, 10% glycerol, 5 mM EDTA, 1 mM Na_3VO_4, and 0.5 mM DTT), and the lysates were preincubated with nProtein A–Sepharose Fast Flow (GE Healthcare #17528002) for 1 h at 4 °C. After centrifugation, supernatants were incubated with nProtein A–Sepharose Fast Flow and specific antibodies for 4 h at 4 °C, and then the beads were washed twice with wash buffer (500 mM NaCl, 50 mM HEPES, pH 7.5, 1% Nonidet P-40, 10% glycerol, and 0.5 mM DTT) and with lysis buffer. Last, the precipitates were boiled in SDS sample buffer (62.5 mM Tris-HCl, pH 6.8, 5% 2-mercaptoethanol, 2% SDS, 5% sucrose, and 0.005% bromphenol blue) for 5 min at 97 °C. Immunoprecipitates and lysates were immunoblotted as described previously (52).

Protein purification

GST fusion proteins were expressed in *E. coli* BL-21 strain. After initial incubation, 0.2 mM isopropyl β-D-thiogalactopyranoside was added, and the cells were incubated for another 18 h at 18 °C. Cells expressing GST fusion proteins were lysed in lysis buffer (150 mM NaCl, 50 mM Tris-HCl, pH 7.4, 1% Nonidet P-40, 1 mM DTT, 1 mM phenylmethylsulfonyl fluoride, 3 μg/ml pepstatin, 10 μg/ml leupeptin, and 10 μM E-64) and incubated with GSH-Sepharose-4B (GE Healthcare #17075601) for 2 h at 4 °C. GST tag was removed using PreScission Protease (GE Healthcare #27084301) in a buffer containing 50 mM Tris-HCl (pH 7.4), 150 mM NaCl, and 1 mM DTT, and proteins were finally dialyzed (using Spectra/Por dialysis tubing, Spectrum #129015) into a buffer containing 50 mM MES (pH 6.6), 5 mM DTT, 1 mM EGTA, and 5 mM $MgSO_4$. To confirm purification, the obtained proteins were separated using SDS-PAGE and analyzed through Coomassie Brilliant Blue (CBB) staining (Rapid Stain CBB Kit, Nacalai Tesque #30035-14).

In vitro MT polymerization assay

In vitro MT polymerization was performed as described previously (53). Briefly, 12.5 μM tubulin and 2 μM recombinant CEP104 TOG domain protein were incubated for 15 min on ice in assembly buffer (50 mM MES, pH 6.6, 3.4 M glycerol, 5 mM DTT, 1 mM EGTA, 5 mM $MgSO_4$, and 1 mM GTP), and then 100-μl aliquots of samples were pipetted into cold 96-well plates. Next, the plates were moved to a Styrofoam water box and floated on water at 25 °C for 1 min and then immediately placed into a Benchmark Plus microplate reader (Bio-Rad), which was prewarmed at 37 °C. Scattering was monitored at 350 nm in 10-s intervals over 1500 s. Minimum A_{350} was used for baseline adjustment.

Quantitative RT-PCR

Total RNA was isolated from RPE1 cells by using an Isogen II kit (Nippon Gene #311-07361), and then 1 μg of total RNA was reverse-transcribed to obtain single-stranded cDNA by using a PrimeScript RT reagent kit (TaKaRa #RR037A). For quantitative PCR, cDNA fragments were amplified using SYBR Premix Ex Taq II (TaKaRa #RR081A), and the products were detected using an Applied Biosystems 7300 system (Thermo Fisher Scientific). All reactions were performed as per the manufacturer's instructions. The sequences of the primers for quantitative PCR were as follows: 5′-CAGGGAGTGCAGCCAATACAG-3′ (*Gli1* forward primer), 5′-GAGCGGCGGCTACAGTATA-3′ (*Gli1* reverse primer), 5′-ATTTGGTCGCGGTTCTTG-3′ (*UBC* forward primer), and 5′-TGCCTTGACATTCTC-GATGGT-3′ (*UBC* reverse primer). Data were analyzed using 7300 System Software (Thermo Fisher Scientific) and Microsoft Excel (Microsoft).

Statistical analysis

Data are expressed as scatter dot plots from more than three independent experiments. All statistical analyses were performed using Prism 8 (GraphPad Software), and p values were calculated using ordinary one-way ANOVA followed by Tukey's test for multiple-data set comparisons.

Data availability

All of the data described in this study are contained within the article.

Acknowledgments—We thank T. Kubota (Tohoku University) for technical assistance, and Drs. K. Ohashi and K. Yasumoto (Tohoku University), Dr. M. Nishita (Fukushima Medical University), and Dr. S. Chiba (Osaka City University) for helpful advice and encouragement. We also thank Dr. T. Inoue (Johns Hopkins University), Dr. B. D. Dynlacht (New York University), and Dr. K. Nakayama (Kyoto University) for providing cDNA plasmids encoding EB1, CP110, and GST-tagged anti-GFP-nanobody; Dr. I. Wada (Fukushima Medical University) for letting us use an A1 confocal microscope; and Dr. H. Nakanishi (Kumamoto University) for providing hTERT-RPE1 cells.

Author contributions—T. Y. and T. N. resources; T. Y., T. N., S. U., and Y. S. data curation; T. Y., T. N., S. U., and Y. S. formal analysis; T. Y. and T. N. validation; T. Y., T. N., S. U., and Y. S. investigation; T. Y. and T. N.visualization; T. Y. and T. N. methodology; T. N. and K. M. conceptualization; T. N. and K. M. supervision; T. N. and K. M. funding acquisition; T. N. and K. M. writing-original draft; T. N. and K. M. project administration; K. M. writing-review and editing.

Funding and additional information—This work was supported by Grants-in-aid for Scientific Research 15H04347 and 18H02398 (to K. M.) and 16K20910 (to T. N.) from the Japan Society for the Promotion of Science (JSPS), KAKENHI.

Conflict of interest—The authors declare that they have no conflicts of interest with the contents of this article.

Abbreviations—The abbreviations used are: MT, microtubule; Ac, acetylated; CEP104, centrosomal protein of 104 kDa; CEP97, centrosomal protein of 97 kDa; CP110, centrosomal protein of 110 kDa; CSPP1, centrosome and spindle pole–associated protein 1; EB1, end-binding protein 1; GST, glutathione *S*-transferase; GPR161, G-protein–coupled receptor 161; Hh, Hedgehog; IF, immunofluorescence; IFT, intraflagellar transport; IP, immunoprecipitation; JBTS, Joubert syndrome; JR, jelly-roll; NEK1, NIMA-

related kinase-1; RPE, retinal pigment epithelial; SAG, Smo agonist; sr, siRNA-resistant; Smo, Smoothened; TOG, tumor-overexpressed gene; WB, Western blot; YFP, yellow fluorescent protein; ZF, zinc-finger; DAPI, 4′,6-diamino-2-phenylindole; FCS, fetal calf serum; CBB, Coomassie Brilliant Blue; ANOVA, analysis of variance.

References

1. Gerdes, J. M., Davis, E. E., and Katsanis, N. (2009) The vertebrate primary cilium in development, homeostasis, and disease. *Cell* **137,** 32–45 CrossRef Medline
2. Seeley, E. S., and Nachury, M. V. (2010) The perennial organelle: assembly and disassembly of the primary cilium. *J. Cell Sci.* **123,** 511–518 CrossRef Medline
3. Kobayashi, T., and Dynlacht, B. D. (2011) Regulating the transition from centriole to basal body. *J. Cell Biol.* **193,** 435–444 CrossRef Medline
4. Spektor, A., Tsang, W. Y., Khoo, D., and Dynlacht, B. D. (2007) Cep97 and CP110 suppress a cilia assembly program. *Cell* **130,** 678–690 CrossRef Medline
5. Kim, S., and Dynlacht, B. D. (2013) Assembling a primary cilium. *Curr. Opin. Cell Biol.* **25,** 506–511 CrossRef Medline
6. Sánchez, I., and Dynlacht, B. D. (2016) Cilium assembly and disassembly. *Nat. Cell Biol.* **18,** 711–717 CrossRef Medline
7. Izawa, I., Goto, H., Kasahara, K., and Inagaki, M. (2015) Current topics of functional links between primary cilia and cell cycle. *Cilia* **4,** 12 CrossRef Medline
8. Ishikawa, H., and Marshall, W. F. (2011) Ciliogenesis: building the cell's antenna. *Nat. Rev. Mol. Cell Biol.* **12,** 222–234 CrossRef Medline
9. Avasthi, P., and Marshall, W. F. (2012) Stages of ciliogenesis and regulation of ciliary length. *Differentiation* **83,** S30–S42 CrossRef Medline
10. Nakayama, K., and Katoh, Y. (2018) Ciliary protein trafficking mediated by IFT and BBSome complexes with the aid of kinesin-2 and dynein-2 motors. *J. Biochem.* **163,** 155–164 CrossRef Medline
11. Nachury, M. V., and Mick, D. U. (2019) Establishing and regulating the composition of cilia for signal transduction. *Nat. Rev. Mol. Cell Biol.* **20,** 389–405 CrossRef Medline
12. Ishikawa, H., and Marshall, W. F. (2017) Intraflagellar transport and ciliary dynamics. *Cold Spring Harb. Perspect. Biol.* **9,** a021998 CrossRef Medline
13. Wallingford, J. B., and Mitchell, B. (2011) Strange as it may seem: the many links between Wnt signaling, planar cell polarity, and cilia. *Genes Dev.* **25,** 201–213 CrossRef Medline
14. Mukhopadhyay, S., and Rohatgi, R. (2014) G-protein-coupled receptors, Hedgehog signaling and primary cilia. *Semin. Cell Dev. Biol.* **33,** 63–72 CrossRef Medline
15. Basten, S. G., and Giles, R. H. (2013) Functional aspects of primary cilia in signaling, cell cycle and tumorigenesis. *Cilia* **2,** 6 CrossRef Medline
16. Goetz, S. C., and Anderson, K. V. (2010) The primary cilium: a signalling centre during vertebrate development. *Nat. Rev. Genet.* **11,** 331–344 CrossRef Medline
17. Fliegauf, M., Benzing, T., and Omran, H. (2007) When cilia go bad: cilia defects and ciliopathies. *Nat. Rev. Mol. Cell Biol.* **8,** 880–893 CrossRef Medline
18. Romani, M., Micalizzi, A., and Valente, E. M. (2013) Joubert syndrome: congenital cerebellar ataxia with the molar tooth. *Lancet Neurol.* **12,** 894–905 CrossRef Medline
19. Shi, X., Garcia, G., Van De Weghe, J. C., McGorty, R., Pazour, G. J., Doherty, D., Huang, B., and Reiter, J. F. (2017) Super-resolution microscopy reveals that disruption of ciliary transition-zone architecture causes Joubert syndrome. *Nat. Cell Biol.* **19,** 1178–1188 CrossRef Medline
20. Chih, B., Liu, P., Chinn, Y., Chalouni, C., Komuves, L. G., Hass, P. E., Sandoval, W., and Peterson, A. S. (2011) A ciliopathy complex at the transition zone protects the cilia as a privileged membrane domain. *Nat. Cell Biol.* **14,** 61–72 CrossRef Medline
21. Nozaki, S., Katoh, Y., Terada, M., Michisaka, S., Funabashi, T., Takahashi, S., Kontani, K., and Nakayama, K. (2017) Regulation of ciliary retrograde protein trafficking by the Joubert syndrome proteins ARL13B and INPP5E. *J. Cell Sci.* **130,** 563–576 CrossRef Medline
22. Dafinger, C., Liebau, M. C., Elsayed, S. M., Hellenbroich, Y., Boltshauser, E., Korenke, G. C., Fabretti, F., Janecke, A. R., Ebermann, I., Nürnberg, G., Nürnberg, P., Zentgraf, H., Koerber, F., Addicks, K., Elsobky, E., *et al.* (2011) Mutations in KIF7 link Joubert syndrome with Sonic Hedgehog signaling and microtubule dynamics. *J. Clin. Invest.* **121,** 2662–2667 CrossRef Medline
23. Liem, K. F., He, M., Ocbina, P. J. R., and Anderson, K. V. (2009) Mouse Kif7/Costal2 is a cilia-associated protein that regulates Sonic hedgehog signaling. *Proc. Natl. Acad. Sci. U. S. A.* **106,** 13377–13382 CrossRef Medline
24. Larkins, C. E., Gonzalez Aviles, G. D., East, M. P., Kahn, R. A., and Caspary, T. (2011) Arl13b regulates ciliogenesis and the dynamic localization of Shh signaling proteins. *Mol. Biol. Cell* **22,** 4694–4703 CrossRef Medline
25. Shimada, H., Lu, Q., Insinna-Kettenhofen, C., Nagashima, K., English, M. A., Semler, E. M., Mahgerefteh, J., Cideciyan, A. V., Li, T., Brooks, B. P., Gunay-Aygun, M., Jacobson, S. G., Cogliati, T., Westlake, C. J., and Swaroop, A. (2017) *In vitro* modeling using ciliopathy-patient-derived cells reveals distinct cilia dysfunctions caused by CEP290 mutations. *Cell Rep.* **20,** 384–396 CrossRef Medline
26. Dyson, J. M., Conduit, S. E., Feeney, S. J., Hakim, S., DiTommaso, T., Fulcher, A. J., Sriratana, A., Ramm, G., Horan, K. A., Gurung, R., Wicking, C., Smyth, I., and Mitchell, C. A. (2017) INPP5E regulates phosphoinositide-dependent cilia transition zone function. *J. Cell Biol.* **216,** 247–263 CrossRef Medline
27. Srour, M., Hamdan, F. F., McKnight, D., Davis, E., Mandel, H., Schwartzentruber, J., Martin, B., Patry, L., Nassif, C., Dionne-Laporte, A., Ospina, L. H., Lemyre, E., Massicotte, C., Laframboise, R., Maranda, B., *et al.* (2015) Joubert syndrome in French Canadians and identification of mutations in CEP104. *Am. J. Hum. Genet.* **97,** 744–753 CrossRef Medline
28. Luo, M., Cao, L., Cao, Z., Ma, S., Shen, Y., Yang, D., Lu, C., Lin, Z., Liu, Z., Yu, Y., Cai, R., Chen, C., Gao, H., Wang, X., Cao, M., *et al.* (2019) Whole exome sequencing reveals novel CEP104 mutations in a Chinese patient with Joubert syndrome. *Mol. Genet. Genomic Med.* **7,** e1004 CrossRef Medline
29. Jiang, K., Toedt, G., Montenegro Gouveia, S., Davey, N. E., Hua, S., Van Der Vaart, B., Grigoriev, I., Larsen, J., Pedersen, L. B., Bezstarosti, K., Lince-Faria, M., Demmers, J., Steinmetz, M. O., Gibson, T. J., and Akhmanova, A. (2012) A proteome-wide screen for mammalian SxIP motif-containing microtubule plus-end tracking proteins. *Curr. Biol.* **22,** 1800–1807 CrossRef Medline
30. Satish Tammana, T. V., Tammana, D., Diener, D. R., and Rosenbaum, J. (2013) Centrosomal protein CEP104 (*Chlamydomonas* FAP256) moves to the ciliary tip during ciliary assembly. *J. Cell Sci.* **126,** 5018–5029 CrossRef Medline
31. Louka, P., Vasudevan, K. K., Guha, M., Joachimiak, E., Wloga, D., Tomasi, R. F. X., Baroud, C. N., Dupuis-Williams, P., Galati, D. F., Pearson, C. G., Rice, L. M., Moresco, J. J., Yates, J. R., Jiang, Y. Y., Lechtreck, K., *et al.* (2018) Proteins that control the geometry of microtubules at the ends of cilia. *J. Cell Biol.* **217,** 4298–4313 CrossRef Medline
32. Al-Jassar, C., Andreeva, A., Barnabas, D. D., McLaughlin, S. H., Johnson, C. M., Yu, M., and van Breugel, M. (2017) The ciliopathy-associated Cep104 protein interacts with tubulin and Nek1 kinase. *Structure* **25,** 146–156 CrossRef Medline
33. Rezabkova, L., Kraatz, S. H. W., Akhmanova, A., Steinmetz, M. O., and Kammerer, R. A. (2016) Biophysical and structural characterization of the centriolar protein CEP104 interaction network. *J. Biol. Chem.* **291,** 18496–18504 CrossRef Medline
34. Frikstad, K.-A. M., Molinari, E., Thoresen, M., Ramsbottom, S. A., Hughes, F., Letteboer, S. J. F., Gilani, S., Schink, K. O., Stokke, T., Geimer, S., Pedersen, L. B., Giles, R. H., Akhmanova, A., Roepman, R., Sayer, J. A., *et al.* (2019) A CEP104-CSPP1 complex is required for formation of primary cilia competent in Hedgehog signaling. *Cell Rep.* **28,** 1907–1922.e6 CrossRef Medline
35. Al-Bassam, J., and Chang, F. (2011) Regulation of microtubule dynamics by TOG-domain proteins XMAP215/Dis1 and CLASP. *Trends Cell Biol.* **21,** 604–614 CrossRef Medline

36. Schrøder, J. M., Larsen, J., Komarova, Y., Akhmanova, A., Thorsteinsson, R. I., Grigoriev, I., Manguso, R., Christensen, S. T., Pedersen, S. F., Geimer, S., and Pedersen, L. B. (2011) EB1 and EB3 promote cilia biogenesis by several centrosome-related mechanisms. *J. Cell Sci.* **124,** 2539–2551 CrossRef Medline
37. Pedersen, L. B., Geimer, S., Sloboda, R. D., and Rosenbaum, J. L. (2003) The microtubule plus end-tracking protein EB1 is localized to the flagellar tip and basal bodies in *Chlamydomonas reinhardtii*. *Curr. Biol.* **13,** 1969–1974 CrossRef Medline
38. Gupta, G. D., Coyaud, É., Gonçalves, J., Mojarad, B. A., Liu, Y., Wu, Q., Gheiratmand, L., Comartin, D., Tkach, J. M., Cheung, S. W. T., Bashkurov, M., Hasegan, M., Knight, J. D., Lin, Z.-Y., Schueler, M., *et al.* (2015) A dynamic protein interaction landscape of the human centrosome-cilium interface. *Cell* **163,** 1484–1499 CrossRef Medline
39. Schmidt, T. I., Kleylein-Sohn, J., Westendorf, J., Le Clech, M., Lavoie, S. B., Stierhof, Y. D., and Nigg, E. A. (2009) Control of centriole length by CPAP and CP110. *Curr. Biol.* **19,** 1005–1011 CrossRef Medline
40. Kohlmaier, G., Lončarek, J., Meng, X., McEwen, B. F., Mogensen, M. M., Spektor, A., Dynlacht, B. D., Khodjakov, A., and Gönczy, P. (2009) Overly long centrioles and defective cell division upon excess of the SAS-4-related protein CPAP. *Curr. Biol.* **19,** 1012–1018 CrossRef Medline
41. Kobayashi, T., Tsang, W. Y., Li, J., Lane, W., and Dynlacht, B. D. (2011) Centriolar kinesin Kif24 interacts with CP110 to remodel microtubules and regulate ciliogenesis. *Cell* **145,** 914–925 CrossRef Medline
42. Bangs, F. K., Schrode, N., Hadjantonakis, A. K., and Anderson, K. V. (2015) Lineage specificity of primary cilia in the mouse embryo. *Nat. Cell Biol.* **17,** 113–122 CrossRef Medline
43. Chen, J. K., Taipale, J., Young, K. E., Maiti, T., and Beachy, P. A. (2002) Small molecule modulation of smoothened activity. *Proc. Natl. Acad. Sci. U. S. A.* **99,** 14071–14076 CrossRef Medline
44. Pal, K., Hwang, S. h., Somatilaka, B., Badgandi, H., Jackson, P. K., DeFea, K., and Mukhopadhyay, S. (2016) Smoothened determines β-arrestin-mediated removal of the G protein-coupled receptor Gpr161 from the primary cilium. *J. Cell Biol.* **212,** 861–875 CrossRef Medline
45. Mukhopadhyay, S., Wen, X., Ratti, N., Loktev, A., Rangell, L., Scales, S. J., and Jackson, P. K. (2013) The ciliary G-protein-coupled receptor Gpr161 negatively regulates the Sonic hedgehog pathway via cAMP signaling. *Cell* **152,** 210–223 CrossRef Medline
46. Aher, A., Kok, M., Sharma, A., Rai, A., Olieric, N., Rodriguez-Garcia, R., Katrukha, E. A., Weinert, T., Olieric, V., Kapitein, L. C., Steinmetz, M. O., Dogterom, M., and Akhmanova, A. (2018) CLASP suppresses microtubule catastrophes through a single TOG domain. *Dev. Cell* **46,** 40–58.e8 CrossRef Medline
47. Caspary, T., Larkins, C. E., and Anderson, K. V. (2007) The graded response to Sonic Hedgehog depends on cilia architecture. *Dev. Cell* **12,** 767–778 CrossRef Medline
48. Pusapati, G. V., Kong, J. H., Patel, B. B., Krishnan, A., Sagner, A., Kinnebrew, M., Briscoe, J., Aravind, L., and Rohatgi, R. (2018) CRISPR screens uncover genes that regulate target cell sensitivity to the morphogen Sonic Hedgehog. *Dev. Cell* **44,** 113–129.e8 CrossRef Medline
49. Breslow, D. K., Hoogendoorn, S., Kopp, A. R., Morgens, D. W., Vu, B. K., Kennedy, M. C., Han, K., Li, A., Hess, G. T., Bassik, M. C., Chen, J. K., and Nachury, M. V. (2018) A CRISPR-based screen for Hedgehog signaling provides insights into ciliary function and ciliopathies. *Nat. Genet.* **50,** 460–471 CrossRef Medline
50. Eguether, T., San Agustin, J. T., Keady, B. T., Jonassen, J. A., Liang, Y., Francis, R., Tobita, K., Johnson, C. A., Abdelhamed, Z. A., Lo, C. W., and Pazour, G. J. (2014) IFT27 links the BBSome to IFT for maintenance of the ciliary signaling compartment. *Dev. Cell* **31,** 279–290 CrossRef Medline
51. Bhogaraju, S., Taschner, M., Morawetz, M., Basquin, C., and Lorentzen, E. (2011) Crystal structure of the intraflagellar transport complex 25/27. *EMBO J.* **30,** 1907–1918 CrossRef Medline
52. Nagai, T., Ikeda, M., Chiba, S., Kanno, S., and Mizuno, K. (2013) Furry promotes acetylation of microtubules in the mitotic spindle by inhibition of SIRT2 tubulin deacetylase. *J. Cell Sci.* **126,** 4369–4380 CrossRef Medline
53. Slep, K. C., and Vale, R. D. (2007) Structural basis of microtubule plus end tracking by XMAP215, CLIP-170, and EB1. *Mol. Cell* **27,** 976–991 CrossRef Medline